Acta Cryst E CRYSTALLOGRAPHIC COMMUNICATIONS
ISSN 2056-9890

Structural characterization of the azoxy derivative of an antitubercular 8-nitro-1,3-benzothiazin-4-one[1]

Adrian Richter,[a] Richard Goddard,[b] Peter Imming[a] and Rüdiger W. Seidel[a]*

[a]Martin-Luther-Universität Halle-Wittenberg, Institut für Pharmazie, Wolfgang-Langenbeck-Str. 4, 06120 Halle (Saale), Germany, and [b]Max-Planck-Institut für Kohlenforschung, Kaiser-Wilhelm-Platz 1, 45470 Mülheim an der Ruhr, Germany. *Correspondence e-mail: ruediger.seidel@pharmazie.uni-halle.de

Received 4 November 2022
Accepted 11 November 2022

Edited by B. Therrien, University of Neuchâtel, Switzerland

[1] Dedicated to Professor George M. Sheldrick on the occasion of his 80th birthday.

Keywords: benzothiazinones; azoxy compound; antituberculosis drugs; reaction mechanism; crystal structure.

CCDC reference: 2219153

Supporting information: this article has supporting information at journals.iucr.org/e

(*Z*)-1,2-Bis[4-oxo-2-(piperidin-1-yl)-6-(trifluoromethyl)-4*H*-benzo[*e*][1,3]thiazin-8-yl]diazene oxide, $C_{28}H_{24}F_6N_6O_3S_2$, was obtained and its structure determined while attempting to crystallize and structurally characterize 8-nitro-2-(piperidin-1-yl)-6-(trifluoromethyl)-4*H*-benzo[*e*][1,3]thiazin-4-one, a simplified analogue of the antituberculosis clinical drug candidate BTZ043. X-ray crystallography revealed the structure of the azoxy compound to be comprised of two benzothiazinone moieties linked by a *Z*-configured azoxy group in an almost coplanar arrangement. In the crystal, the molecules are densely packed, revealing a herringbone pattern.

1. Chemical context

8-Nitro-1,3-benzothiazin-4-ones (BTZs) are a class of covalently binding inhibitors of decaprenylphosphoryl-β-D-ribose-2′-epimerase (DprE1), an enzyme crucial for cell-wall synthesis in *Mycobacterium tuberculosis*, the primary pathogen causing tuberculosis (Chikhale *et al.*, 2018). BTZ043 (Fig. 1; Makarov *et al.*, 2009) is one of the most advanced candidates and has recently completed a Phase Ib/IIa clinical study (ClinicalTrials.gov Identifier: NCT04044001). Compound **1** (Fig. 1) represents a simplified analogue of BTZ043, lacking the spiroketal moiety (Richter *et al.*, 2018). The generally accepted mechanism of action of BTZs is a reduction of the nitro group to a nitroso group by $FADH_2$, followed by a semimercaptal formation with Cys387 (Trefzer *et al.*, 2010, 2012; Neres *et al.*, 2012; Richter *et al.*, 2018). Tiwari *et al.* (2013) suggested an alternative mechanism in which the reduction to the nitroso form is initiated by nucleophilic addition of thiolate to C-7 of the BTZ system. Subsequent formation of the azoxy form was postulated, but no proof of the structure is available. Liu *et al.* (2019) reported detection of the BTZ043

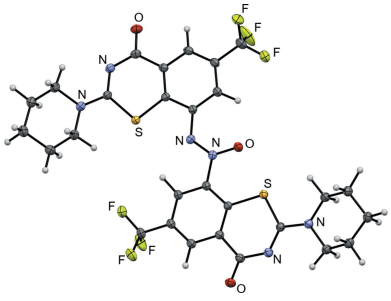

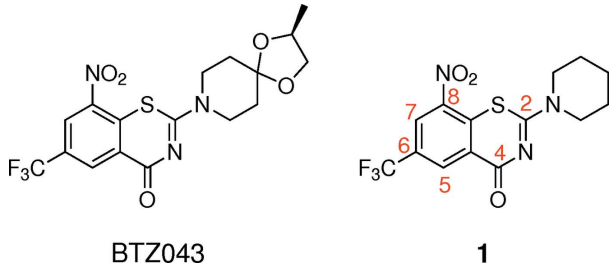

Figure 1
Chemical diagrams of BTZ043 and **1**, showing the systematic numbering scheme for the BTZ system.

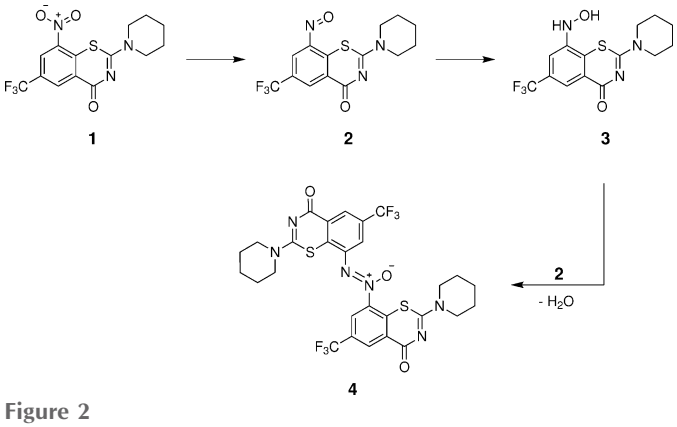

Figure 2
Possible reduction pathway leading from **1** to **4** in DMF in the presence of moisture (see text).

azoxy form by LC/MS in a reaction mixture. To the best of our knowledge, an azoxy derivative of an antitubercular BTZ has not been structurally characterized thus far.

The azoxy derivative of **1** was obtained unintentionally during an attempt to grow crystals of **1** for X-ray crystallography by leaving a dimethylformamide (DMF) solution of **1** at ambient conditions and allowing the solvent to evaporate slowly. Fig. 2 shows a possible reaction pathway to the azoxy derivative. Compound **1** is reduced to the nitroso congener **2** and then to the hydroxylamine **3**, which reacts with excess of **2** in a condensation reaction to yield the azoxy compound **4**. Although it remains unclear how the reduction of the nitro group in **1** was induced in the absence of an intended reducing agent, this pathway has some plausibility (Chen *et al.*, 2017; Cole *et al.*, 2017). Possibly DMF acted as a reducing agent here (Heravi *et al.*, 2018). Moreover, DMF usually contains small amounts of water, which causes partial hydrolysis (Meglitskii & Kvasha, 1972). Thus, trace amounts of dimethylamine often contained in DMF may have initiated reduction of **1** by nucleophilic addition to C-7 of the BTZ system. A related reaction of BTZs with nucleophilic attack by thiolates on C-7 was postulated by Tiwari *et al.* (2013).

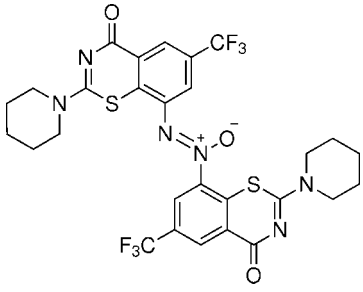

The identification and structural characterization of **4** could be relevant for drug stability assessment of BTZs. To the best of our knowledge, targeted synthesis of an azoxy derivative of an antitubercular BTZ and antimycobacterial testing has not been reported so far. In this context, it is interesting to note that a variety of azoxy compounds occur naturally and have various biological effects, including potent growth inhibition of *M. tuberculosis in vitro* exerted by the compound elaiomycin (Dembitsky *et al.*, 2017; Wibowo & Ding, 2020).

Table 1
Selected bond angles (°).

N2—C10—C11	112.23 (9)	N2′—C10′—C11′	110.86 (10)
C12—C11—C10	111.03 (10)	C12′—C11′—C10′	111.95 (10)
C13—C12—C11	108.02 (9)	C13′—C12′—C11′	109.74 (10)
C14—C13—C12	111.74 (9)	C14′—C13′—C12′	110.73 (11)
N2—C14—C13	111.16 (9)	N2′—C14′—C13′	110.78 (9)
C14—N2—C10	114.52 (8)	C14′—N2′—C10′	113.32 (9)

2. Structural commentary

Fig. 3 shows the molecular structure of **4** in the crystal. The two benzothiazinone moieties and the *Z*-configured azoxy linkage exhibit a nearly planar structure. The dihedral angles between the mean plane of the azoxy group (*i.e.* N1′, N1 and O2) and the mean planes of the attached benzene rings are 6.7 (1)° for the ring C4*A*–C8*A* and 5.4 (1)° for the ring C4*A*′–C8*A*′. The tilt angle between the mean planes of the two benzene rings is 4.15 (6)°. The planar conformation is assumed to be the ground state, possibly stabilized by intramolecular C—S···O and C—S···N chalcogen bonds (Scilabra *et al.*, 2019). Additional stabilization, however, does not appear to be necessary, considering that (*Z*)-azoxybenzene (diphenyldiazene oxide) is planar in the gas phase, as revealed by electron diffraction and *ab initio* calculations (Tsuji *et al.*, 2000) but not in the crystal (*vide infra*). The piperidine rings attached to C-2 of the BTZ system both adopt a low-energy chair conformation with slight distortions from the ideal tetrahedral angle (Table 1). The azoxy oxygen atom O2 has a significant effect on an otherwise symmetrical hypothetical azo-BTZ structure, with the N1′—C8′ distance at 1.394 (1) Å being notably shorter than the N1—C8 distance of 1.459 (1) Å and a clear geometry change at the C-8 position. The difference between the two parts of the molecule is highlighted in Fig. 4, which shows a superposition of the benzene rings of the BTZ moieties of two identical molecules.

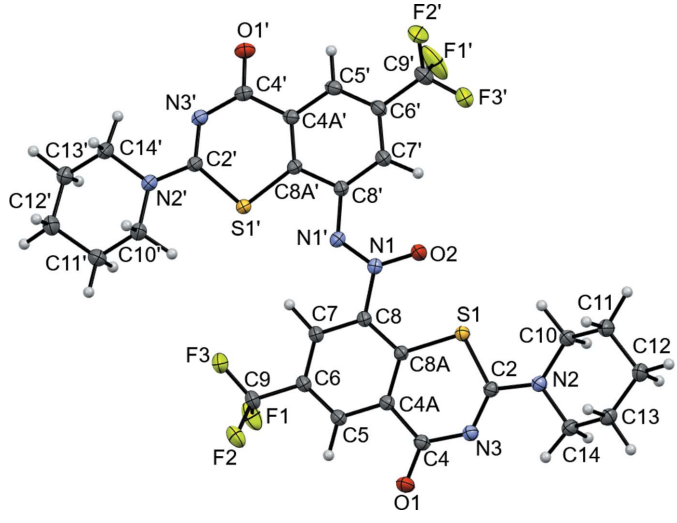

Figure 3
Displacement ellipsoid plot (50% probability level) of **4**. H atoms are shown as small spheres of arbitrary radius.

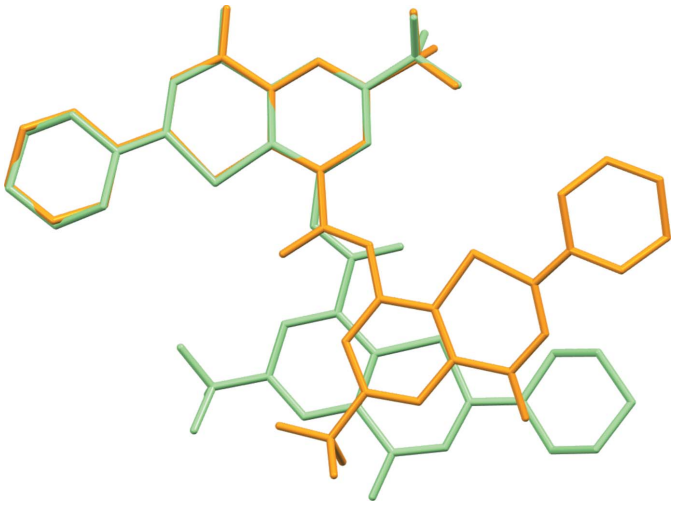

Figure 4
Superposition of the benzene rings of the benzothiazinone moieties of two identical molecules (green and orange), illustrating the difference in the attachment of the azoxy group to C8 and C8′ in the two parts of **4**.

3. Supramolecular features

In the crystal structure, the molecules are densely packed, as revealed by a packing index of 73.0% (Kitaigorodskii, 1973), which was calculated with *PLATON* (Spek, 2020). A view of the crystal structure along the [101] direction reveals a herringbone pattern (Fig. 5). The separation between the planes of stacked molecules is *ca* 3.31 Å, similar to the interplanar distance in graphite (3.35 Å; Delhaes, 2001). As can be seen in the crystal structure, the trifluoromethyl groups of adjacent molecules are in close proximity to one another, but no intermolecular F···F contacts shorter than the sum of the corresponding van der Waals radii (Bondi, 1964) are encountered.

4. Database survey

A search of the Cambridge Structural Database (CSD; Groom *et al.*, 2016) *via* the WebCSD interface (CCDC, 2017) in October of 2022 revealed no structure of an azoxy-BTZ, but four structures of 8-nitro-BTZs, *viz.* BTZ043 (CSD refcodes: HACQOY and HACQOV01; Richter *et al.*, 2022*a*) and its 5-methyl derivative (MELLAU; Richter *et al.*, 2022*b*), macozinone (PBTZ169; LOPXAS; Zhang & Aldrich, 2019) and 2-(4-Boc-piperazin-1-yl)-8-nitro-6-(trifluoromethyl)-BTZ (MESSOW; Richter *et al.*, 2022*c*), with an average C_{BTZ}—N_{nitro} bond length of 1.46 (1) Å. This can be compared with the C8—N1 bond length of 1.459 (1) and the C8′—N1′ bond length of 1.394 (1) Å in **4**, which highlights the short C8′—N1′ bond length resulting from O2 being bonded to N1.

A substructure search for variously substituted acyclic azoxybenzene moieties yielded more than a hundred hits. Almost half of these have dihedral angles between the phenyl rings of less than 20°, although there are exceptions such as 1,3-dimethoxy-2-(phenylazoxy)benzene (VUNSII; Zhang *et al.*, 2015) with a dihedral angle between the aromatic rings of *ca* 90°, illustrating that packing and steric effects are sufficient to disturb the ground-state conformation. The simplest azoxybenzene structure is that of (*Z*)-azoxybenzene (TIHTEK; Gonzáles Martínez & Bernès, 2007). The structure most related to that of **4**, containing bicycles with fused six-membered rings, appears to be that of (*Z*)-1,2-bis[2-(2,2,2-trifluoroacetyl)naphthalen-1-yl]diazene oxide (XOZHUS; Belligund *et al.*, 2019). In contrast to **4**, in both TIHTEK and XOZHUS the aromatic rings are not coplanar and are significantly tilted out of the plane of the azoxy group. This can be reasonably attributed to effects of crystal packing in TIHTEK and steric effects of the substituents in *ortho*-position to the azoxy group in XOZHUS.

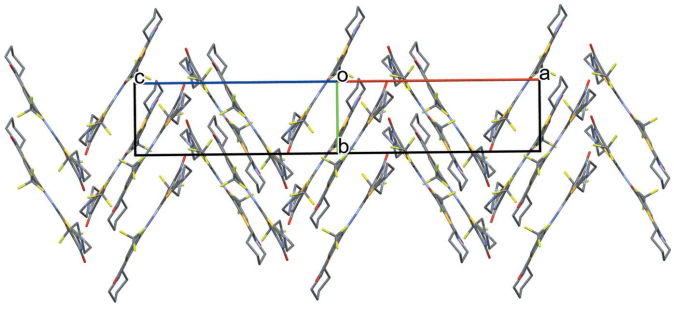

Figure 5
Projection of the crystal structure of **4** in the [101] direction. H atoms are omitted for clarity.

5. Synthesis and crystallization

The synthesis of **1** is described elsewhere (Richter *et al.*, 2018). DMF was of reagent-grade quality. Crystals of **4** suitable for single-crystal X-ray diffraction were obtained from a solution of **1** in DMF at room temperature, when the solvent was allowed to evaporate slowly over a period of several weeks.

6. Refinement

The crystal structure was initially refined to convergence by standard independent atom model (IAM) refinement with *SHELXL* (Sheldrick, 2015*b*). The final structure refinement was performed with Hirshfeld atom refinement (HAR), using aspherical scattering factors with *NoSpherA2* (Kleemiss *et al.*, 2021; Midgley *et al.*, 2021) partitioning in *OLEX2* (Dolomanov *et al.*, 2009) based on electron density from iterative single determinant SCF single-point DFT calculations using *ORCA* (Neese *et al.*, 2020) with a B3LYP functional (Becke, 1993; Lee *et al.*, 1988) and a def2-TZVPP basis set. Fig. 6 depicts the F_{calc}(HAR)–F_{calc}(IAM) deformation density map, showing the modelled deformation of the electron density as a result of bonding between independent spherical atoms. Crystal data, data collection and structure refinement details are summarized in Table 2.

Table 2
Experimental details.

Crystal data	
Chemical formula	$C_{28}H_{24}F_6N_6O_3S_2$
M_r	670.66
Crystal system, space group	Monoclinic, $P2_1/c$
Temperature (K)	100
a, b, c (Å)	24.0754 (8), 6.3343 (2), 19.6822 (8)
β (°)	113.1511 (14)
V (Å^3)	2759.84 (17)
Z	4
Radiation type	Mo $K\alpha$
μ (mm^{-1})	0.28
Crystal size (mm)	0.06 × 0.05 × 0.03
Data collection	
Diffractometer	Bruker AXS D8 Venture
Absorption correction	Gaussian (*SADABS*; Krause *et al.*, 2015)
T_{min}, T_{max}	0.990, 0.996
No. of measured, independent and observed [$I \geq 2u(I)$] reflections	178787, 8391, 7021
R_{int}	0.070
Refinement	
$R[F^2 > 2\sigma(F^2)]$, $wR(F^2)$, S	0.030, 0.080, 1.06
No. of reflections	8391
No. of parameters	502
H-atom treatment	All H-atom parameters refined
$\Delta\rho_{max}$, $\Delta\rho_{min}$ (e Å^{-3})	0.51, −0.42

Computer programs: *APEX4* (Bruker, 2017), *SAINT* (Bruker, 2019), SHELXT (Sheldrick, 2015*a*), *OLEX2.refine* (Bourhis *et al.*, 2015), *Mercury* (Macrae *et al.*, 2020), *OLEX2* (Dolomanov *et al.*, 2009) and *publCIF* (Westrip, 2010).

Acknowledgements

We would like to thank Dr Thomas Weyhermüller for providing measurement time at the X-ray diffraction facility of the Max-Planck-Institut für Chemische Energiekonversion (Mülheim an der Ruhr, Germany), and Heike Schucht and Elke Dreher for technical assistance. We acknowledge the financial support within the funding programme Open Access Publishing by the German Research Foundation (DFG).

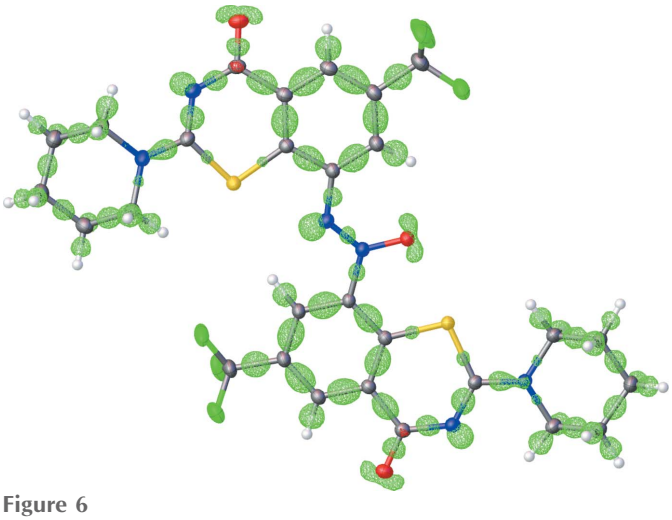

Figure 6
The F_{calc}(HAR)–F_{calc}(IAM) deformation density map superimposed on the molecular structure of **4** (map level: 0.2 e Å^{-3}). Colour scheme: C grey, H white, N blue, O red, S yellow.

References

Becke, A. D. (1993). *J. Chem. Phys.* **98**, 5648–5652.
Belligund, K., Mathew, T., Hunt, J. R., Nirmalchandar, A., Haiges, R., Dawlaty, J. & Prakash, G. K. S. (2019). *J. Am. Chem. Soc.* **141**, 15921–15931.
Bondi, A. (1964). *J. Phys. Chem.* **68**, 441–451.
Bourhis, L. J., Dolomanov, O. V., Gildea, R. J., Howard, J. A. K. & Puschmann, H. (2015). *Acta Cryst.* A**71**, 59–75.
Bruker (2017). *APEX4*. Bruker AXS Inc., Madison, Wisconsin, USA.
Bruker (2019). *SAINT*. Bruker AXS Inc., Madison, Wisconsin, USA.
CCDC (2017). CSD web interface – intuitive, cross-platform, web-based access to CSD data. Cambridge Crystallographic Data Centre, 12 Union Road, Cambridge, UK.
Chen, Y.-F., Chen, J., Lin, L.-J. & Chuang, G. J. (2017). *J. Org. Chem.* **82**, 11626–11630.
Chikhale, R. V., Barmade, M. A., Murumkar, P. R. & Yadav, M. R. (2018). *J. Med. Chem.* **61**, 8563–8593.
Cole, K. P., Johnson, M. D., Laurila, M. E. & Stout, J. R. (2017). *React. Chem. Eng.* **2**, 288–294.
Delhaes, P. (2001). *Graphite and Precursors.* London: CRC Press.
Dembitsky, V. M., Gloriozova, T. A. & Poroikov, V. V. (2017). *Nat. Prod. Bioprospect.* **7**, 151–169.
Dolomanov, O. V., Bourhis, L. J., Gildea, R. J., Howard, J. A. K. & Puschmann, H. (2009). *J. Appl. Cryst.* **42**, 339–341.
González Martínez, S. P. & Bernès, S. (2007). *Acta Cryst.* E**63**, o3639.
Groom, C. R., Bruno, I. J., Lightfoot, M. P. & Ward, S. C. (2016). *Acta Cryst.* B**72**, 171–179.
Heravi, M. M., Ghavidel, M. & Mohammadkhani, L. (2018). *RSC Adv.* **8**, 27832–27862.
Kitaigorodskii, A. I. (1973). *Molecular crystals and molecules.* London: Academic Press.
Kleemiss, F., Dolomanov, O. V., Bodensteiner, M., Peyerimhoff, N., Midgley, M., Bourhis, L. J., Genoni, A., Malaspina, L. A., Jayatilaka, D., Spencer, J. L., White, F., Grundkötter-Stock, B., Steinhauer, S., Lentz, D., Puschmann, H. & Grabowsky, S. (2021). *Chem. Sci.* **12**, 1675–1692.
Krause, L., Herbst-Irmer, R., Sheldrick, G. M. & Stalke, D. (2015). *J. Appl. Cryst.* **48**, 3–10.
Lee, C., Yang, W. & Parr, R. G. (1988). *Phys. Rev. B*, **37**, 785–789.
Liu, R., Krchnak, V., Brown, S. N. & Miller, M. J. (2019). *ACS Med. Chem. Lett.* **10**, 1462–1466.
Macrae, C. F., Sovago, I., Cottrell, S. J., Galek, P. T. A., McCabe, P., Pidcock, E., Platings, M., Shields, G. P., Stevens, J. S., Towler, M. & Wood, P. A. (2020). *J. Appl. Cryst.* **53**, 226–235.
Makarov, V., Manina, G., Mikusova, K., Möllmann, U., Ryabova, O., Saint-Joanis, B., Dhar, N., Pasca, M. R., Buroni, S., Lucarelli, A. P., Milano, A., De Rossi, E., Belanova, M., Bobovska, A., Dianiskova, P., Kordulakova, J., Sala, C., Fullam, E., Schneider, P., McKinney, J. D., Brodin, P., Christophe, T., Waddell, S., Butcher, P., Albrethsen, J., Rosenkrands, I., Brosch, R., Nandi, V., Bharath, S., Gaonkar, S., Shandil, R. K., Balasubramanian, V., Balganesh, T., Tyagi, S., Grosset, J., Riccardi, G. & Cole, S. T. (2009). *Science*, **324**, 801–804.
Meglitskii, V. A. & Kvasha, N. M. (1972). *Fibre Chem.* **3**, 327–329.
Midgley, L., Bourhis, L. J., Dolomanov, O. V., Grabowsky, S., Kleemiss, F., Puschmann, H. & Peyerimhoff, N. (2021). *J. Chem. Phys.* **152**, 224108.
Neese, F., Wennmohs, F., Becker, U. & Riplinger, C. (2020). *J. Chem. Phys.* **152**, 224108.
Neres, J., Pojer, F., Molteni, E., Chiarelli, L. R., Dhar, N., Boy-Röttger, S., Buroni, S., Fullam, E., Degiacomi, G., Lucarelli, A. P., Read, R. J., Zanoni, G., Edmondson, D. E., De Rossi, E., Pasca, M. R., McKinney, J. D., Dyson, P. J., Riccardi, G., Mattevi, A., Cole, S. T. & Binda, C. (2012). *Sci. Transl. Med.* **4**, 150r, a121.
Richter, A., Narula, G., Rudolph, I., Seidel, R. W., Wagner, C., Av-Gay, Y. & Imming, P. (2022*c*). *ChemMedChem*, **17**, e202100733.
Richter, A., Patzer, M., Goddard, R., Lingnau, J. B., Imming, P. & Seidel, R. W. (2022*a*). *J. Mol. Struct.* **1248**, 131419.

Richter, A., Rudolph, I., Möllmann, U., Voigt, K., Chung, C., Singh, O. M. P., Rees, M., Mendoza-Losana, A., Bates, R., Ballell, L., Batt, S., Veerapen, N., Fütterer, K., Besra, G., Imming, P. & Argyrou, A. (2018). *Sci. Rep.* **8**, 13473.
Richter, A., Seidel, R. W., Graf, J., Goddard, R., Lehmann, C., Schlegel, T., Khater, N. & Imming, P. (2022*b*). *ChemMedChem*, **17**, e202200021.
Scilabra, P., Terraneo, G. & Resnati, G. (2019). *Acc. Chem. Res.* **52**, 1313–1324.
Sheldrick, G. M. (2015*a*). *Acta Cryst.* A**71**, 3–8.
Sheldrick, G. M. (2015*b*). *Acta Cryst.* C**71**, 3–8.
Spek, A. L. (2020). *Acta Cryst.* E**76**, 1–11.
Tiwari, R., Moraski, G. C., Krchňák, V., Miller, P. A., Colon-Martinez, M., Herrero, E., Oliver, A. G. & Miller, M. J. (2013). *J. Am. Chem. Soc.* **135**, 3539–3549.
Trefzer, C., Rengifo-Gonzalez, M., Hinner, M. J., Schneider, P., Makarov, V., Cole, S. T. & Johnsson, K. (2010). *J. Am. Chem. Soc.* **132**, 13663–13665.
Trefzer, C., Škovierová, H., Buroni, S., Bobovská, A., Nenci, S., Molteni, E., Pojer, F., Pasca, M. R., Makarov, V., Cole, S. T., Riccardi, G., Mikušová, K. & Johnsson, K. (2012). *J. Am. Chem. Soc.* **134**, 912–915.
Tsuji, T., Takashima, H., Takeuchi, H., Egawa, T. & Konaka, S. (2000). *J. Mol. Struct.* **554**, 203–210.
Westrip, S. P. (2010). *J. Appl. Cryst.* **43**, 920–925.
Wibowo, M. & Ding, L. (2020). *J. Nat. Prod.* **83**, 3482–3491.
Zhang, G. & Aldrich, C. C. (2019). *Acta Cryst.* C**75**, 1031–1035.
Zhang, D., Cui, X., Yang, F., Zhang, Q., Zhu, Y. & Wu, Y. (2015). *Org. Chem. Front.* **2**, 951–955.

supporting information

Acta Cryst. (2022). E**78**, 1244-1248 [https://doi.org/10.1107/S2056989022010842]

Structural characterization of the azoxy derivative of an antitubercular 8-nitro-1,3-benzothiazin-4-one

Adrian Richter, Richard Goddard, Peter Imming and Rüdiger W. Seidel

Computing details

Data collection: *APEX4* (Bruker, 2017); cell refinement: *SAINT* (Bruker, 2019); data reduction: *SAINT* (Bruker, 2019); program(s) used to solve structure: SHELXT (Sheldrick, 2015a); program(s) used to refine structure: *olex2.refine* (Bourhis *et al.*, 2015); molecular graphics: *Mercury* (Macrae *et al.*, 2020) and OLEX2 (Dolomanov *et al.*, 2009); software used to prepare material for publication: *publCIF* (Westrip, 2010).

(*Z*)-1,2-Bis[4-oxo-2-(piperidin-1-yl)-6-(trifluoromethyl)-4*H*-benzo[e][1,3]thiazin-8-yl]diazene oxide

Crystal data

$C_{28}H_{24}F_6N_6O_3S_2$
M_r = 670.66
Monoclinic, $P2_1/c$
a = 24.0754 (8) Å
b = 6.3343 (2) Å
c = 19.6822 (8) Å
β = 113.1511 (14)°
V = 2759.84 (17) Å^3
Z = 4
$F(000)$ = 1378.110
D_x = 1.614 Mg m^{-3}
Mo $K\alpha$ radiation, λ = 0.71073 Å
Cell parameters from 9921 reflections
θ = 2.3–30.4°
μ = 0.28 mm^{-1}
T = 100 K
Prism, yellow
0.06 × 0.05 × 0.03 mm

Data collection

Bruker AXS D8 Venture diffractometer
Radiation source: IμS
Incoatec Helios mirrors monochromator
Detector resolution: 7.391 pixels mm^{-1}
φ– and ω–scans
Absorption correction: gaussian (SADABS; Krause *et al.*, 2015)
T_{min} = 0.990, T_{max} = 0.996
178787 measured reflections
8391 independent reflections
7021 reflections with $I \geq 2u(I)$
R_{int} = 0.070
θ_{max} = 30.5°, θ_{min} = 2.3°
h = −39→40
k = −10→10
l = −32→32

Refinement

Refinement on F^2
Least-squares matrix: full
$R[F^2 > 2\sigma(F^2)]$ = 0.030
$wR(F^2)$ = 0.080
S = 1.06
8391 reflections
502 parameters
0 restraints
0 constraints
Primary atom site location: dual
Secondary atom site location: difference Fourier map
Hydrogen site location: difference Fourier map
All H-atom parameters refined
$w = 1/[\sigma^2(F_o^2) + (0.0404P)^2 + 0.5834P]$ where $P = (F_o^2 + 2F_c^2)/3$

$(\Delta/\sigma)_{max}$ = 0.001
$\Delta\rho_{max}$ = 0.51 e Å^{-3}
$\Delta\rho_{min}$ = −0.41 e Å^{-3}

Special details

Experimental. Crystal mounted on a MiTeGen loop using Perfluoropolyether PFO-XR75

Fractional atomic coordinates and isotropic or equivalent isotropic displacement parameters (Å²)

	x	*y*	*z*	U_{iso}*/U_{eq}
C2	0.28147 (4)	1.62528 (16)	0.35880 (6)	0.01856 (18)
C4	0.18168 (5)	1.66757 (16)	0.27097 (6)	0.01990 (19)
C4A	0.18126 (4)	1.46289 (16)	0.23218 (5)	0.01821 (18)
C5	0.12727 (5)	1.41066 (17)	0.17388 (6)	0.02096 (19)
H5	0.0901 (6)	1.516 (2)	0.1592 (8)	0.032 (3)*
C6	0.12223 (4)	1.22486 (18)	0.13493 (6)	0.0215 (2)
C7	0.17143 (5)	1.09111 (17)	0.15219 (6)	0.02065 (19)
H7	0.1706 (7)	0.938 (2)	0.1223 (8)	0.034 (4)*
C8	0.22558 (4)	1.14234 (16)	0.20994 (5)	0.01785 (18)
C8A	0.23135 (4)	1.32656 (15)	0.25264 (5)	0.01688 (17)
C9	0.06319 (5)	1.1574 (2)	0.07626 (6)	0.0285 (2)
C10	0.38359 (5)	1.58701 (17)	0.45870 (6)	0.0233 (2)
H10a	0.3900 (6)	1.455 (2)	0.4242 (8)	0.032 (3)*
H10b	0.3783 (7)	1.516 (3)	0.5073 (9)	0.046 (4)*
C11	0.43872 (5)	1.72905 (19)	0.48551 (7)	0.0287 (2)
H11a	0.4441 (7)	1.795 (3)	0.4356 (9)	0.044 (4)*
H11b	0.4809 (8)	1.628 (3)	0.5181 (10)	0.054 (5)*
C12	0.43017 (5)	1.91406 (19)	0.52990 (7)	0.0284 (2)
H12a	0.4223 (7)	1.856 (2)	0.5775 (9)	0.045 (4)*
H12b	0.4717 (8)	2.017 (3)	0.5496 (9)	0.050 (4)*
C13	0.37393 (5)	2.03337 (17)	0.48121 (6)	0.0244 (2)
H13a	0.3795 (7)	2.092 (2)	0.4309 (9)	0.044 (4)*
H13b	0.3658 (7)	2.169 (2)	0.5094 (8)	0.042 (4)*
C14	0.31845 (5)	1.89287 (17)	0.45499 (7)	0.0245 (2)
H14a	0.3085 (7)	1.838 (3)	0.5017 (9)	0.049 (4)*
H14b	0.2788 (7)	1.972 (2)	0.4171 (8)	0.042 (4)*
F3	0.07072 (4)	1.02538 (16)	0.02812 (5)	0.0534 (3)
S1	0.297929 (11)	1.37714 (4)	0.329373 (14)	0.01863 (6)
N1	0.27597 (4)	0.99673 (14)	0.22486 (5)	0.01818 (16)
N2	0.32766 (4)	1.70422 (14)	0.41709 (5)	0.02082 (17)
N3	0.23098 (4)	1.73330 (14)	0.33002 (5)	0.02101 (17)
O1	0.13567 (3)	1.77651 (13)	0.24771 (5)	0.02728 (17)
O2	0.32334 (3)	1.03059 (13)	0.28039 (4)	0.02664 (17)
F1	0.02873 (3)	1.05970 (15)	0.10561 (5)	0.0451 (2)
F2	0.03113 (3)	1.32047 (13)	0.03808 (4)	0.03864 (18)
C2′	0.20796 (5)	0.37012 (16)	−0.00025 (6)	0.02017 (19)
C4′	0.29718 (5)	0.18587 (16)	0.07323 (6)	0.02048 (19)
C4A′	0.32046 (4)	0.35975 (16)	0.12869 (6)	0.01907 (18)
C5′	0.37853 (5)	0.33989 (18)	0.18380 (6)	0.0223 (2)

H5′	0.4033 (7)	0.204 (2)	0.1849 (8)	0.044 (4)*
C6′	0.40175 (5)	0.49576 (18)	0.23691 (6)	0.0229 (2)
C7′	0.36784 (5)	0.67241 (18)	0.23859 (6)	0.0218 (2)
H7′	0.3860 (6)	0.787 (2)	0.2804 (8)	0.034 (3)*
C8′	0.30904 (4)	0.69248 (16)	0.18499 (5)	0.01844 (18)
C8A′	0.28619 (4)	0.53676 (16)	0.12859 (5)	0.01775 (18)
C9′	0.46319 (5)	0.4618 (2)	0.29701 (7)	0.0313 (3)
C10′	0.11963 (5)	0.56488 (19)	−0.09017 (7)	0.0272 (2)
H10c	0.1317 (7)	0.647 (3)	−0.1305 (9)	0.051 (4)*
H10d	0.1259 (7)	0.666 (3)	−0.0433 (9)	0.046 (4)*
C11′	0.05376 (5)	0.4965 (2)	−0.12664 (7)	0.0288 (2)
H11c	0.0264 (8)	0.638 (3)	−0.1484 (10)	0.055 (5)*
H11d	0.0421 (8)	0.432 (3)	−0.0822 (10)	0.055 (5)*
C12′	0.04379 (6)	0.3354 (2)	−0.18782 (7)	0.0306 (2)
H12c	−0.0026 (7)	0.282 (3)	−0.2089 (9)	0.051 (4)*
H12d	0.0532 (7)	0.410 (3)	−0.2314 (9)	0.047 (4)*
C13′	0.08662 (5)	0.1495 (2)	−0.15767 (7)	0.0285 (2)
H13c	0.0763 (7)	0.070 (2)	−0.1158 (8)	0.040 (4)*
H13d	0.0819 (7)	0.034 (3)	−0.2003 (9)	0.047 (4)*
C14′	0.15169 (5)	0.2246 (2)	−0.12305 (7)	0.0326 (3)
H14c	0.1830 (8)	0.097 (3)	−0.0982 (10)	0.058 (5)*
H14d	0.1662 (7)	0.307 (3)	−0.1646 (9)	0.048 (4)*
N1′	0.26622 (4)	0.84787 (14)	0.17848 (5)	0.02021 (17)
N2′	0.15965 (4)	0.38055 (16)	−0.06438 (5)	0.0264 (2)
N3′	0.24492 (4)	0.20906 (14)	0.01250 (5)	0.02222 (18)
O1′	0.32738 (4)	0.02386 (12)	0.08251 (5)	0.02674 (17)
F1′	0.46238 (4)	0.29899 (17)	0.33958 (6)	0.0656 (3)
F2′	0.50496 (3)	0.42022 (16)	0.27055 (5)	0.0510 (2)
F3′	0.48340 (3)	0.62741 (14)	0.34161 (4)	0.04065 (19)
S1′	0.214168 (11)	0.58337 (4)	0.060830 (14)	0.01939 (6)

Atomic displacement parameters (Å²)

	U^{11}	U^{22}	U^{33}	U^{12}	U^{13}	U^{23}
C2	0.0182 (4)	0.0166 (4)	0.0206 (4)	−0.0010 (3)	0.0073 (4)	−0.0014 (3)
C4	0.0183 (4)	0.0184 (5)	0.0224 (5)	0.0012 (3)	0.0074 (4)	0.0007 (4)
C4A	0.0168 (4)	0.0189 (4)	0.0185 (4)	0.0009 (3)	0.0065 (4)	0.0003 (3)
C5	0.0168 (4)	0.0242 (5)	0.0197 (5)	0.0023 (4)	0.0049 (4)	−0.0002 (4)
C6	0.0164 (4)	0.0258 (5)	0.0193 (4)	0.0010 (4)	0.0037 (4)	−0.0027 (4)
C7	0.0173 (4)	0.0231 (5)	0.0187 (4)	0.0009 (4)	0.0040 (4)	−0.0030 (4)
C8	0.0161 (4)	0.0194 (4)	0.0167 (4)	−0.0004 (3)	0.0049 (4)	−0.0013 (3)
C8A	0.0163 (4)	0.0174 (4)	0.0165 (4)	0.0004 (3)	0.0059 (3)	0.0003 (3)
C9	0.0189 (5)	0.0349 (6)	0.0236 (5)	0.0025 (4)	−0.0002 (4)	−0.0064 (4)
C10	0.0216 (5)	0.0196 (5)	0.0256 (5)	0.0009 (4)	0.0059 (4)	−0.0030 (4)
C11	0.0210 (5)	0.0289 (6)	0.0319 (6)	0.0006 (4)	0.0058 (4)	−0.0100 (5)
C12	0.0245 (5)	0.0265 (5)	0.0281 (6)	0.0004 (4)	0.0037 (4)	−0.0077 (4)
C13	0.0270 (5)	0.0184 (5)	0.0255 (5)	−0.0004 (4)	0.0080 (4)	−0.0038 (4)
C14	0.0221 (5)	0.0219 (5)	0.0283 (5)	0.0003 (4)	0.0087 (4)	−0.0062 (4)

F3	0.0275 (4)	0.0711 (6)	0.0430 (5)	0.0112 (4)	−0.0060 (3)	−0.0325 (4)
S1	0.01677 (11)	0.01686 (11)	0.01941 (11)	0.00039 (8)	0.00407 (9)	−0.00168 (8)
N1	0.0181 (4)	0.0188 (4)	0.0167 (4)	0.0000 (3)	0.0059 (3)	−0.0013 (3)
N2	0.0188 (4)	0.0184 (4)	0.0236 (4)	−0.0001 (3)	0.0066 (3)	−0.0032 (3)
N3	0.0191 (4)	0.0189 (4)	0.0236 (4)	0.0009 (3)	0.0070 (3)	−0.0022 (3)
O1	0.0219 (4)	0.0233 (4)	0.0316 (4)	0.0060 (3)	0.0052 (3)	−0.0016 (3)
O2	0.0203 (4)	0.0250 (4)	0.0275 (4)	0.0034 (3)	0.0017 (3)	−0.0062 (3)
F1	0.0247 (4)	0.0540 (5)	0.0443 (5)	−0.0130 (3)	0.0005 (3)	0.0029 (4)
F2	0.0277 (4)	0.0455 (5)	0.0299 (4)	0.0071 (3)	−0.0024 (3)	0.0017 (3)
C2′	0.0196 (4)	0.0202 (5)	0.0210 (5)	0.0005 (4)	0.0082 (4)	−0.0040 (4)
C4′	0.0222 (5)	0.0180 (5)	0.0236 (5)	0.0022 (4)	0.0116 (4)	0.0004 (4)
C4A′	0.0185 (4)	0.0197 (4)	0.0198 (4)	0.0027 (4)	0.0084 (4)	0.0014 (4)
C5′	0.0195 (5)	0.0241 (5)	0.0236 (5)	0.0053 (4)	0.0088 (4)	0.0024 (4)
C6′	0.0177 (4)	0.0284 (5)	0.0207 (5)	0.0044 (4)	0.0055 (4)	0.0018 (4)
C7′	0.0178 (4)	0.0256 (5)	0.0196 (5)	0.0021 (4)	0.0047 (4)	−0.0016 (4)
C8′	0.0172 (4)	0.0206 (5)	0.0166 (4)	0.0008 (3)	0.0057 (4)	−0.0004 (3)
C8A′	0.0180 (4)	0.0185 (4)	0.0175 (4)	0.0011 (3)	0.0078 (4)	−0.0007 (3)
C9′	0.0208 (5)	0.0376 (6)	0.0294 (6)	0.0072 (5)	0.0033 (5)	0.0008 (5)
C10′	0.0273 (5)	0.0273 (5)	0.0219 (5)	0.0038 (4)	0.0041 (4)	−0.0051 (4)
C11′	0.0249 (5)	0.0316 (6)	0.0262 (5)	0.0075 (4)	0.0063 (4)	−0.0017 (5)
C12′	0.0249 (5)	0.0327 (6)	0.0277 (6)	0.0004 (5)	0.0031 (5)	−0.0053 (5)
C13′	0.0244 (5)	0.0290 (6)	0.0288 (6)	−0.0002 (4)	0.0069 (5)	−0.0085 (5)
C14′	0.0230 (5)	0.0381 (7)	0.0329 (6)	0.0021 (5)	0.0068 (5)	−0.0178 (5)
N1′	0.0214 (4)	0.0211 (4)	0.0177 (4)	0.0020 (3)	0.0073 (3)	−0.0030 (3)
N2′	0.0222 (4)	0.0290 (5)	0.0244 (5)	0.0040 (4)	0.0052 (4)	−0.0095 (4)
N3′	0.0223 (4)	0.0197 (4)	0.0248 (4)	0.0013 (3)	0.0093 (4)	−0.0043 (3)
O1′	0.0291 (4)	0.0196 (4)	0.0319 (4)	0.0058 (3)	0.0124 (3)	0.0006 (3)
F1′	0.0411 (5)	0.0661 (7)	0.0601 (6)	0.0001 (5)	−0.0119 (4)	0.0341 (5)
F2′	0.0201 (3)	0.0722 (6)	0.0523 (5)	0.0090 (4)	0.0053 (3)	−0.0254 (5)
F3′	0.0266 (4)	0.0545 (5)	0.0303 (4)	0.0095 (3)	−0.0002 (3)	−0.0110 (3)
S1′	0.01745 (11)	0.02073 (12)	0.01844 (11)	0.00258 (9)	0.00539 (9)	−0.00378 (9)

Geometric parameters (Å, º)

C2—S1	1.7730 (10)	N1—N1′	1.2685 (12)
C2—N2	1.3416 (13)	C2′—N2′	1.3402 (14)
C2—N3	1.3135 (13)	C2′—N3′	1.3115 (13)
C4—C4A	1.5026 (14)	C2′—S1′	1.7750 (10)
C4—N3	1.3595 (13)	C4′—C4A′	1.4958 (15)
C4—O1	1.2304 (12)	C4′—N3′	1.3604 (14)
C4A—C5	1.3938 (14)	C4′—O1′	1.2291 (12)
C4A—C8A	1.4074 (13)	C4A′—C5′	1.3981 (14)
C5—H5	1.063 (14)	C4A′—C8A′	1.3917 (13)
C5—C6	1.3837 (15)	C5′—H5′	1.041 (16)
C6—C7	1.3855 (14)	C5′—C6′	1.3858 (16)
C6—C9	1.4987 (15)	C6′—C7′	1.3931 (15)
C7—H7	1.129 (15)	C6′—C9′	1.5027 (15)
C7—C8	1.3899 (14)	C7′—H7′	1.053 (14)

C8—C8A	1.4127 (14)	C7′—C8′	1.3994 (14)
C8—N1	1.4589 (13)	C8′—C8A′	1.4240 (14)
C8A—S1	1.7461 (10)	C8′—N1′	1.3943 (13)
C9—F3	1.3284 (14)	C8A′—S1′	1.7475 (10)
C9—F1	1.3347 (15)	C9′—F1′	1.3336 (16)
C9—F2	1.3310 (14)	C9′—F2′	1.3280 (15)
C10—H10a	1.124 (14)	C9′—F3′	1.3313 (15)
C10—H10b	1.108 (16)	C10′—H10c	1.082 (16)
C10—C11	1.5162 (16)	C10′—H10d	1.082 (16)
C10—N2	1.4724 (13)	C10′—C11′	1.5239 (17)
C11—H11a	1.120 (16)	C10′—N2′	1.4712 (15)
C11—H11b	1.158 (18)	C11′—H11c	1.094 (17)
C11—C12	1.5234 (16)	C11′—H11d	1.098 (17)
C12—H12a	1.089 (15)	C11′—C12′	1.5240 (17)
C12—H12b	1.129 (17)	C12′—H12c	1.082 (16)
C12—C13	1.5173 (16)	C12′—H12d	1.080 (16)
C13—H13a	1.114 (16)	C12′—C13′	1.5231 (17)
C13—H13b	1.081 (15)	C13′—H13c	1.076 (15)
C13—C14	1.5168 (15)	C13′—H13d	1.086 (16)
C14—H14a	1.095 (16)	C13′—C14′	1.5182 (16)
C14—H14b	1.077 (16)	C14′—H14c	1.080 (18)
C14—N2	1.4709 (13)	C14′—H14d	1.135 (16)
N1—O2	1.2494 (11)	C14′—N2′	1.4740 (14)

N2—C2—S1	113.15 (7)	C4—N3—C2	123.92 (9)
N3—C2—S1	127.50 (8)	N3′—C2′—N2′	119.40 (9)
N3—C2—N2	119.35 (9)	S1′—C2′—N2′	114.27 (8)
N3—C4—C4A	121.86 (9)	S1′—C2′—N3′	126.32 (8)
O1—C4—C4A	118.01 (9)	N3′—C4′—C4A′	120.89 (9)
O1—C4—N3	120.13 (10)	O1′—C4′—C4A′	118.45 (10)
C5—C4A—C4	116.16 (9)	O1′—C4′—N3′	120.62 (10)
C8A—C4A—C4	123.38 (9)	C5′—C4A′—C4′	118.26 (9)
C8A—C4A—C5	120.45 (9)	C8A′—C4A′—C4′	122.71 (9)
H5—C5—C4A	119.2 (7)	C8A′—C4A′—C5′	119.01 (10)
C6—C5—C4A	120.55 (10)	H5′—C5′—C4A′	118.7 (8)
C6—C5—H5	120.3 (7)	C6′—C5′—C4A′	120.32 (10)
C7—C6—C5	120.27 (9)	C6′—C5′—H5′	120.9 (8)
C9—C6—C5	121.30 (10)	C7′—C6′—C5′	121.59 (10)
C9—C6—C7	118.36 (10)	C9′—C6′—C5′	118.16 (10)
H7—C7—C6	124.0 (8)	C9′—C6′—C7′	120.08 (10)
C8—C7—C6	119.63 (10)	H7′—C7′—C6′	120.2 (8)
C8—C7—H7	116.4 (8)	C8′—C7′—C6′	118.92 (10)
C8A—C8—C7	121.38 (9)	C8′—C7′—H7′	120.9 (8)
N1—C8—C7	117.09 (9)	C8A′—C8′—C7′	119.41 (9)
N1—C8—C8A	121.53 (8)	N1′—C8′—C7′	128.73 (9)
C8—C8A—C4A	117.63 (9)	N1′—C8′—C8A′	111.85 (8)
S1—C8A—C4A	121.80 (8)	C8′—C8A′—C4A′	120.65 (9)
S1—C8A—C8	120.55 (7)	S1′—C8A′—C4A′	123.16 (8)

F3—C9—C6	112.03 (9)	S1′—C8A′—C8′	116.19 (7)
F1—C9—C6	111.19 (10)	F1′—C9′—C6′	110.62 (10)
F1—C9—F3	107.41 (11)	F2′—C9′—C6′	112.50 (10)
F2—C9—C6	112.17 (10)	F2′—C9′—F1′	107.08 (11)
F2—C9—F3	107.29 (10)	F3′—C9′—C6′	113.43 (10)
F2—C9—F1	106.44 (10)	F3′—C9′—F1′	106.67 (11)
H10b—C10—H10a	108.0 (11)	F3′—C9′—F2′	106.14 (10)
C11—C10—H10a	109.9 (7)	H10d—C10′—H10c	110.6 (12)
C11—C10—H10b	108.8 (8)	C11′—C10′—H10c	108.7 (9)
N2—C10—H10a	110.6 (7)	C11′—C10′—H10d	109.9 (8)
N2—C10—H10b	107.1 (8)	N2′—C10′—H10c	108.0 (9)
N2—C10—C11	112.23 (9)	N2′—C10′—H10d	108.7 (8)
H11a—C11—C10	107.7 (8)	N2′—C10′—C11′	110.86 (10)
H11b—C11—C10	108.8 (9)	H11c—C11′—C10′	107.8 (9)
H11b—C11—H11a	108.3 (12)	H11d—C11′—C10′	106.0 (9)
C12—C11—C10	111.03 (10)	H11d—C11′—H11c	108.3 (12)
C12—C11—H11a	107.6 (8)	C12′—C11′—C10′	111.95 (10)
C12—C11—H11b	113.2 (9)	C12′—C11′—H11c	110.9 (9)
H12a—C12—C11	110.1 (8)	C12′—C11′—H11d	111.6 (9)
H12b—C12—C11	110.0 (9)	H12c—C12′—C11′	109.3 (9)
H12b—C12—H12a	109.3 (12)	H12d—C12′—C11′	108.4 (8)
C13—C12—C11	108.02 (9)	H12d—C12′—H12c	109.8 (12)
C13—C12—H12a	107.2 (8)	C13′—C12′—C11′	109.74 (10)
C13—C12—H12b	112.2 (9)	C13′—C12′—H12c	110.4 (9)
H13a—C13—C12	109.9 (8)	C13′—C12′—H12d	109.2 (8)
H13b—C13—C12	111.6 (8)	H13c—C13′—C12′	109.7 (8)
H13b—C13—H13a	107.4 (11)	H13d—C13′—C12′	111.8 (9)
C14—C13—C12	111.74 (9)	H13d—C13′—H13c	106.8 (12)
C14—C13—H13a	106.9 (8)	C14′—C13′—C12′	110.73 (11)
C14—C13—H13b	109.2 (8)	C14′—C13′—H13c	108.1 (8)
H14a—C14—C13	110.8 (9)	C14′—C13′—H13d	109.5 (8)
H14b—C14—C13	112.7 (8)	H14c—C14′—C13′	112.5 (9)
H14b—C14—H14a	107.6 (12)	H14d—C14′—C13′	112.1 (8)
N2—C14—C13	111.16 (9)	H14d—C14′—H14c	108.1 (12)
N2—C14—H14a	107.1 (9)	N2′—C14′—C13′	110.78 (9)
N2—C14—H14b	107.2 (8)	N2′—C14′—H14c	107.0 (9)
C8A—S1—C2	101.43 (5)	N2′—C14′—H14d	106.0 (8)
O2—N1—C8	117.93 (8)	C8′—N1′—N1	122.53 (9)
N1′—N1—C8	114.91 (8)	C10′—N2′—C2′	124.91 (9)
N1′—N1—O2	127.16 (9)	C14′—N2′—C2′	120.14 (9)
C10—N2—C2	123.85 (9)	C14′—N2′—C10′	113.32 (9)
C14—N2—C2	119.79 (9)	C4′—N3′—C2′	125.14 (9)
C14—N2—C10	114.52 (8)	C8A′—S1′—C2′	100.51 (5)
C2—N2—C10—C11	144.51 (11)	N1—N1′—C8′—C7′	−1.88 (12)
C2—N2—C14—C13	−143.83 (10)	N1—N1′—C8′—C8A′	176.68 (10)
C2—N3—C4—C4A	−0.99 (12)	C2′—N2′—C10′—C11′	−139.53 (12)
C2—N3—C4—O1	179.08 (10)	C2′—N2′—C14′—C13′	136.81 (12)

C4—C4A—C5—C6	−179.66 (9)	C2′—N3′—C4′—C4A′	−6.44 (12)
C4—C4A—C8A—C8	−177.90 (9)	C2′—N3′—C4′—O1′	175.95 (11)
C4—C4A—C8A—S1	3.77 (11)	C4′—C4A′—C5′—C6′	−179.23 (9)
C4A—C5—C6—C7	−1.77 (12)	C4′—C4A′—C8A′—C8′	176.45 (9)
C4A—C5—C6—C9	174.91 (10)	C4′—C4A′—C8A′—S1′	−3.91 (11)
C4A—C8A—C8—C7	−3.38 (11)	C4A′—C5′—C6′—C7′	1.93 (12)
C4A—C8A—C8—N1	177.15 (8)	C4A′—C5′—C6′—C9′	177.12 (10)
C5—C6—C7—C8	1.37 (12)	C4A′—C8A′—C8′—C7′	3.52 (11)
C5—C6—C9—F3	156.95 (12)	C4A′—C8A′—C8′—N1′	−175.19 (10)
C5—C6—C9—F1	−82.85 (11)	C5′—C6′—C7′—C8′	−0.29 (12)
C5—C6—C9—F2	36.21 (11)	C5′—C6′—C9′—F1′	−65.33 (12)
C6—C7—C8—C8A	1.25 (12)	C5′—C6′—C9′—F2′	54.37 (11)
C6—C7—C8—N1	−179.25 (9)	C5′—C6′—C9′—F3′	174.86 (11)
C7—C8—C8A—S1	174.97 (8)	C6′—C7′—C8′—C8A′	−2.38 (12)
C7—C8—N1—O2	−174.00 (9)	C6′—C7′—C8′—N1′	176.08 (9)
C7—C8—N1—N1′	6.35 (11)	C7′—C8′—C8A′—S1′	−176.14 (8)
C8—N1—N1′—C8′	−178.86 (8)	C10′—C11′—C12′—C13′	54.26 (12)
C10—C11—C12—C13	−57.50 (11)	C10′—N2′—C14′—C13′	−57.05 (11)
C10—N2—C14—C13	51.03 (10)	C11′—C12′—C13′—C14′	−55.55 (12)
C11—C12—C13—C14	58.50 (11)	C12′—C13′—C14′—N2′	56.80 (11)
C12—C13—C14—N2	−55.30 (10)		